Global properties of proton-proton collisions at $\sqrt{s} = 100$ TeV

David d'Enterria[a] **and Tanguy Pierog**[b]

[a]*EP Department, CERN,*
1211 Geneva, Switzerland

[b]*Institut für Kernphysik, Karlsruhe Institute of Technology,*
Postfach 3640, 76021 Karlsruhe, Germany

E-mail: david.d'enterria@cern.ch, tanguy.pierog@kit.edu

ABSTRACT: The global properties of the final states produced in hadronic interactions of protons at centre-of-mass energies of future hadron colliders (such as FCC-hh at CERN, and SppC in China), are studied. The predictions of various Monte Carlo (MC) event generators used in collider physics (PYTHIA 6, PYTHIA 8, and PHOJET) and in ultrahigh-energy cosmic-rays studies (EPOS, and QGSJET) are compared. Despite their different underlying modeling of hadronic interactions, their predictions for proton-proton (p-p) collisions at $\sqrt{s} = 100$ TeV are quite similar. The average of all MC predictions (except PHOJET) for the different observables are: (i) p-p inelastic cross sections $\sigma_{\mathrm{inel}} = 105 \pm 2$ mb; (ii) total charged multiplicity $N_{\mathrm{ch}} = 150 \pm 20$; (iii) charged particle pseudorapidity density at midrapidity $dN_{\mathrm{ch}}/d\eta|_{\eta=0} = 9.6 \pm 0.2$; (iv) energy density at midrapidity $dE/d\eta|_{\eta=0} = 13.6 \pm 1.5$ GeV, and $dE/d\eta|_{\eta=5} = 670 \pm 70$ GeV at the edge of the central region; and (v) average transverse momenta at midrapidities $\langle p_T \rangle = 0.76 \pm 0.07$ GeV/c. At midrapidity, EPOS and QGSJET-II predict larger per-event multiplicity probabilities at very low ($N_{\mathrm{ch}} < 3$) and very high ($N_{\mathrm{ch}} > 100$) particle multiplicities, whereas PYTHIA 6 and 8 feature higher yields in the intermediate region $N_{\mathrm{ch}} \approx 30$–80. These results provide useful information for the estimation of the detector occupancies and energy deposits from pileup collisions at the expected large FCC-hh/SppC luminosities.

Contents

1 Introduction

The Future Circular Collider (FCC) is a post-LHC project in a new 100-km tunnel under consideration at CERN, that would provide hadron and e^+e^- collisions at much higher energies and luminosities than studied so far. Its key scientific goals are the complete exploration of the Higgs sector of the Standard Model (SM), and a significant extension in searches of physics beyond the SM via direct or indirect measurements [1–3]. The FCC-hh will deliver proton-proton (p-p) collisions at a centre-of-mass (c.m.) energy of $\sqrt{s} = 100\,\mathrm{TeV}$ with integrated luminosities at the level of several $100\,\mathrm{fb}^{-1}$ per year or above [4]. Ongoing studies exist on the detector requirements needed to carry out the planned measurements under running conditions involving $\mathcal{O}\,(200 - 1000)$ simultaneous p-p collisions per bunch crossing. Similar studies are under consideration in the context of the Super proton-proton Collider (SppC) promoted by IHEP in China [5]. This work presents a study of the average properties of multiparticle production in p-p collisions at FCC-hh/SppC energies, of usefulness, among others, for the estimation of the expected occupancies and energy deposits in the planned FCC-hh/SppC detectors.

Inclusive particle production in high-energy hadronic collisions receives contributions from "soft" and "hard" interactions, loosely separated by the virtuality of the underlying t-channel exchanges. Soft (hard) processes involve partons of virtualities q^2 typically below (above) a scale $\mathrm{Q}_0^2 \approx 1$–$2\,\mathrm{GeV}$. Semihard parton-parton scatterings around Q_0, dominate the inelastic hadron production cross sections for c.m. energies above a few hundreds GeV, whereas soft scatterings dominate at lower energies ($\sqrt{s} \lesssim 20\,\mathrm{GeV}$) where few hadrons with low transverse momenta $\mathrm{p_T}$ are produced. On the one hand, hard processes can be theoretically described within perturbative Quantum Chromodynamics (pQCD) in a collinear-factorized approach through the convolution of parton distribution functions

(PDFs) and matrix elements for the underlying parton-parton collisions subprocesses. The scattered quarks and gluons produce then collimated bunches of final-state hadrons (jets) through a parton branching process dominated by perturbative splittings described by the Dokshitzer-Gribov-Lipatov-Altarelli-Parisi (DGLAP) equations [6–8], followed by non-perturbative hadronization when the parton virtuality is below $\mathcal{O}\left(1\,\mathrm{GeV}\right)$. On the other hand, soft processes have momenta exchanges not far from $\Lambda_{\mathrm{QCD}} \approx 0.2\,\mathrm{GeV}$ and, although they cannot be treated within pQCD, basic quantum field-theory principles — such as unitarity and analyticity of scattering amplitudes as implemented in Gribov's Reggeon Field Theory (RFT) [9] and exemplified e.g. in the original Dual Parton Model [10] — give a decent account of their cross sections in terms of the exchange of virtual quasi-particle states (Pomerons and Reggeons). Given the extended composite nature of hadrons, even at asymptotically large energies, a non-negligible fraction of inelastic p-p interactions involve soft "peripheral" scatterings. The Pomeron ($\mathbb{P}$) contribution, identified perturbatively with a colour-singlet multigluon exchange, dominates over those from secondary Reggeons (virtual mesons) and is responsible for diffractive dissociation accounting for a noticeable fraction, about a fourth, of the total inelastic cross section at high energies [11, 12].

The general-purpose Monte Carlo (MC) models used in high-energy collider physics, such as PYTHIA 6 [13], PYTHIA 8 [14], HERWIG++ [15], and SHERPA [16], are fully based on a pQCD framework which then incorporates soft diffractive scatterings in a more or less ad hoc manner. In contrast, MC models commonly used in cosmic-ray physics [17] such as EPOS [18–20], QGSJET 01 [21, 22], QGSJET-II [23–26] and SIBYLL [27], as well as PHOJET [28–30] mostly used for collider environments, are fully-based on the RFT approach. The latter MCs start off from a construction of the hadron-hadron elastic scattering amplitude to determine the total, elastic and inelastic (including diffractive) cross sections, extended to include hard processes via "cut (hard) Pomerons" (also known as "parton ladder") diagrams.

At increasingly larger c.m. energies, the inelastic cross section receives major contributions from the region of low parton fractional momenta ($x = p_{\mathrm{parton}}/p_{\mathrm{hadron}}$), where the gluon distribution rises very fast. As a matter of fact, at $\sqrt{s} = 100\,\mathrm{TeV}$ the partonic cross section saturates the total inelastic cross section (i.e. $\sigma_{\mathrm{pQCD}} \approx \sigma_{\mathrm{inel}} \approx 100$ mb) at momenta $\mathrm{p_T} \approx 10\,\mathrm{GeV}/c$, 50 times larger than Λ_{QCD}. Such a "divergent" behaviour (taking place *well* above the infrared regime) is solved by reinterpreting this observation as a consequence of the increasing number of multiparton interactions (MPI) occurring in a single p-p collision. Multiple scattering is naturally incorporated in the RFT models through the "eikonalization" of multi-Pomeron exchanges that unitarize the cross sections, whereas PYTHIA eikonalises multiparton exchanges, supplemented with an impact-parameter (Glauber-like) description of the proton [31]. The energy evolution of such MPI and low-x effects is implemented phenomenologically in all MCs through a transverse momentum cutoff $\mathrm{Q_0}$ of a few GeV that tames the fastly-rising $1/\mathrm{p_T^4}$ minijet cross section (e.g. in PYTHIA the cutoff is introduced through a multiplicative $1/(\mathrm{p_T^2} + \mathrm{Q_0^2})^2$ factor). This $\mathrm{Q_0}$ regulator is often defined so as to run with c.m. energy following a slow power-law (or logarithmic) dependence, closely mimicking the "saturation scale" $\mathrm{Q_{sat}}$ that controls the onset of non-linear (gluon fusion) effects saturating the growth of the PDFs as $x \to 0$ [32]. Last but not least, all MC generators, both based on pQCD or RFT alike, use parton-to-hadron fragmentation

approaches fitted to the experimental data — such as the Lund string [33], area law [34] or cluster hadronization [35] models — to hadronize the coloured degrees of freedom once their virtuality evolves below $\mathcal{O}(1\,\text{GeV})$.

In this paper, we compare the basic properties of the so-called "minimum bias" (MB) observables characterizing the final states produced in proton-proton collisions at $\sqrt{s} = 100\,\text{TeV}$, predicted by pQCD- and RFT-based hadronic interaction models. The MB term refers commonly to inelastic interactions experimentally measured using a generic minimum-bias trigger that accepts a large fraction of the particle production cross section by requiring a minimum activity in one or various detectors. In some cases we present also results for the so-called "non single-diffractive" (NSD) events, mimicking the typical experimental requirement of a two-arm trigger with particles in opposite hemispheres to eliminate backgrounds from beam-gas collisions and cosmic-rays. Such NSD topology reduces significantly the detection rate of (single) diffractive collisions characterized by the survival of one of the colliding protons and particle production in just one hemisphere. The phenomenological setup of our study is described in section 2, the predictions of the different MCs for basic inclusive particle production observables — such as the inelastic cross section σ_{inel}, the particle and energy densities as a function of pseudorapidity $dN_{\text{ch}}/d\eta$ and $dE/d\eta$, the per-event multiplicity distribution $P(N_{\text{ch}})$, and the transverse momentum distribution $dN_{\text{ch}}/dp_{\text{T}}$ (and associated mean transverse momenta $\langle p_{\text{T}} \rangle$) — are presented in section 3, and the main conclusions are summarized in section 4.

2 Theoretical setup

The basic ingredients of the PYTHIA 6 and 8 event generators are leading-order (LO) pQCD $2 \rightarrow 2$ matrix elements, complemented with initial- and final-state parton radiation (ISR and FSR), folded with PDFs (interfaced here via the LHAPDF v6.1.6 package [36]), and the Lund string model for parton hadronization. The decomposition of the inelastic cross section into non-diffractive and diffractive components is based on a Regge model [37]. In this work we use the PYTHIA event generator in two flavours: the Fortran version 6.428 [13], as well as the C++ version PYTHIA 8.17 [14]. We consider two different "tunes" of the parameters governing the non-perturbative and semihard dynamics: ISR and FSR showering, MPI, beam-remnants, FS colour-reconnection, and hadronization. For PYTHIA 6.4 we use the Perugia-350 tune [38], whereas for PYTHIA 8 we use the Monash 2013 tune (Tune:ee=7; Tune:pp=14) [39]. Both sets of parameters (table 1) have been obtained from recent (2011 and 2013 respectively) analysis of MB, underlying-event (UE), and/or Drell-Yan data in p-p collisions at $\sqrt{s} = 7\,\text{TeV}$.

For the initial-state, PYTHIA 6 (Perugia 350) uses the CTEQ5L parton densities [41] and PYTHIA 8 (Monash) the NNPDF2.3 LO set [42], whereas for the description of the transverse parton density, both models use an exponential-of-power profile of the p-p overlap function, $\exp(-r^n)$, with slightly different exponents ($n = 1.7$ and 1.85 respectively). The PYTHIA 6 choice results in a broader p-p overlap which thereby enhances the fluctuations in the number of MPI relative to the Monash-2013 choice. The energy evolution of the MPI cutoff is driven by $Q_0^2(s) = Q_0^2(s_0) \cdot (s/s_0)^\epsilon$, with the parameters quoted in table 1.

Version	Tuning	Diffraction	Semihard dynamics			Initial state		Final state	
	(PYTUNES)		$\sqrt{s_0}$	Q_0	power ϵ	PDF	transv. overlap	colour reconnection	hadronization
6.428	Perugia 2011 (350)	Regge-based [37]	7 TeV	2.93 GeV	0.265	CTEQ5L	$\exp(-r^{1.7})$	strong	Lund model fits (2011)
8.170	Monash 2013 (14)	improved [40]	7 TeV	2.28 GeV	0.215	NNPDF2.3 LO	$\exp(-r^{1.85})$	strong	Lund model fits (2013)

Table 1. Comparison of the various ingredients controlling the non-perturbative and semihard (MPI, parton saturation) dynamics in the two PYTHIA MCs used in this work. See text for details.

Given that the generation of additional parton-parton interactions in the UE is suppressed below Q_0, a *higher* scaling power ϵ implies a *slower* increase of the overall hadronic activity. Thus, the Monash tune results in a slower evolution of Q_0, yielding larger MPI activity at 100 TeV compared to the Perugia tune. The treatment of diffraction has improved in PYTHIA 8 compared to 6. In the former, a diffractive system is viewed as a Pomeron-proton collision, including hard scatterings subject to all the same ISR/FSR and MPI dynamics as for a "normal" parton-parton process [40]. For the final-state, the two tunes have strong final-state colour reconnections (implemented through different models [43, 44]), which act to reduce the number of final-state particles (for a given Q_0 value) or, equivalently, lower the Q_0 value that is required to reach a given average final-state multiplicity. The Lund hadronization parameters for light- and heavy-quarks have been updated in PYTHIA 8 compared to PYTHIA 6 by refitting updated sets of LEP and SLD data [39].

The RFT-based models used in this work differ in various approximations for the collision configurations (e.g. the distributions for the number of cut Pomerons, and for the energy-momentum partition among them), the treatment of diffractive and semihard dynamics, the details of particle production from string fragmentation, and the incorporation or not of other final-state effects (table 2). Whereas the RFT approach is applied using only Pomerons and Reggeons in the case of QGSJET and PHOJET, EPOS extends it to include partonic constituents [45]. In the latter case, this is done with an exact implementation of energy sharing between the different constituents of a hadron at the amplitude level. The evolution of the parton ladders from the projectile and the target side towards the centre (small x) is governed by the DGLAP equations.

For the minijet production cutoff, PHOJET uses dependence of the form $Q_0(s) \sim Q_0 + C \cdot \log(\sqrt{s})$, whereas EPOS and QGSJET-II use a fixed value of Q_0. The latter MC resums dynamically low-x effects through enhanced diagrams corresponding to multi-Pomeron interactions [23, 46, 47]. In that framework, high mass diffraction and parton saturation are related to each other, being governed by the chosen multi-Pomeron vertices, leading to impact-parameter and density-dependent saturation at low momenta [48]. LHC data were used to tune the latest QGSJET-II-04 release [26] shown here. EPOS, on the other hand, uses the wealth of RHIC proton-proton and nucleus-nucleus data to parametrize the low-x behaviour of the parton densities in a more phenomenological way [18] (correcting the $\mathbb{P}$ amplitude used for both cross section and particle production). The EPOS MC is run with the LHC tune [20] which includes collective final-state string interactions which result in an extra radial flow of the final hadrons produced in more central p-p collisions. Among all the MC models presented here, PHOJET is the only one which does not take into account any retuning using LHC data (its last parameter update dates from year 2000).

Model (version)	Diffraction	Semihard dynamics		Final state
		Q_0	Evolution	
EPOS-LHC [20]	effective diffractive $\mathbb{P}$	2.0 GeV	power-law corr. of $\mathbb{P}$	collective flow + area law hadronization
QGSJET-II-04 [23–25]	$\mathbb{P}$ cut-enhanced graphs + G.-W. [49]	1.6 GeV	enhanced $\mathbb{P}$-graphs	simplified string hadronization
PHOJET 1.12 [28, 29]	G.-W. model [49]	2.5 GeV	$Q_0(s) \propto \log(\sqrt{s})$	hadronization via PYTHIA 6.115

Table 2. Comparison of the main ingredients controlling the non-perturbative and semihard dynamics present in the RFT-based event generators used in this work.

The results are presented, in the case of PYTHIA 6 and 8, for primary charged particles, defined as all charged particles produced in the collision including the products of strong and electromagnetic decays but excluding products of weak decays, obtained by decaying all unstable particles[1] for which $c\tau < 10$ mm. For the RFT MCs, unless stated otherwise, the results correspond to the primary charged hadrons (with the same $c\tau$ requirement) but without charged leptons which, nonetheless, represent a very small correction (amounting to about 1.5% of the total charged yield, mostly from the Dalitz π^0 decay). Unless explicitly stated, no requirement on the minimum p_T of the particles is applied in any of the results presented.

3   Results

3.1   Inelastic p-p cross section

The most inclusive quantity measurable in p-p collisions is the total hadronic cross section σ_{tot} and its separation into elastic and inelastic (and, in particular, diffractive) components. In both PYTHIA 6 and 8, the total hadronic cross section is calculated using the Donnachie-Landshoff parametrisation [50], including Pomeron and Reggeon terms, whereas the elastic and diffractive cross sections are calculated using the Schuler-Sjöstrand model [37]. The predictions for the inelastic cross sections in p-p at $\sqrt{s} = 100$ TeV, obtained simply from $\sigma_{\text{tot}} - \sigma_{\text{el}}$, yield basically the same value, $\sigma_{\text{inel}} \approx 107$ mb, for both PYTHIA 6 and 8. The RFT-based MCs, based on $\mathbb{P}$ amplitudes, predict slightly lower values: $\sigma_{\text{inel}} = 105.4, 104.8, 103.1$ mb for EPOS-LHC, QGSJET-II and PHOJET respectively. The $\sqrt{s}$ dependence of the inelastic cross section predictions is shown in figure 1 together with the available data from p-p̄ (UA5 [51], E710 [52] and CDF [53]) and p-p (ALICE [54], ATLAS [55, 56], CMS [57, 58], TOTEM [59–61]) colliders, as well as the AUGER result at $\sqrt{s} = 57$ TeV derived from cosmic-ray data [62]. Interestingly, all model curves cross at about $\sqrt{s} \approx 60$ TeV, and predict about the same inelastic cross section at the nominal FCC-hh/SppC p-p c.m. energy of 100 TeV. A simple average among all predictions yields $\sigma_{\text{inel}}(100\ \text{TeV}) = 105.1 \pm 2.0$ mb, whereas larger differences in the energy evolution of σ_{inel} appear above the $\sqrt{s} \approx 300$ TeV, i.e. around and above the maximum energy observed so far in high-energy cosmic rays impinging on Earth atmosphere [17]. The expected increase in the inelastic p-p cross section at 100 TeV is about 45% compared to the LHC results at 13 TeV ($\sigma_{\text{inel}} = 73.1 \pm 7.7$ mb [56], and (preliminary) 71.3 ± 3.5 mb [58]).

[1]PYTHIA   6.4:   `MSTJ(22)=2,PARJ(71)=10`.   PYTHIA   8:   `ParticleDecays:limitTau0 = on`, `ParticleDecays:tau0Max = 10`.
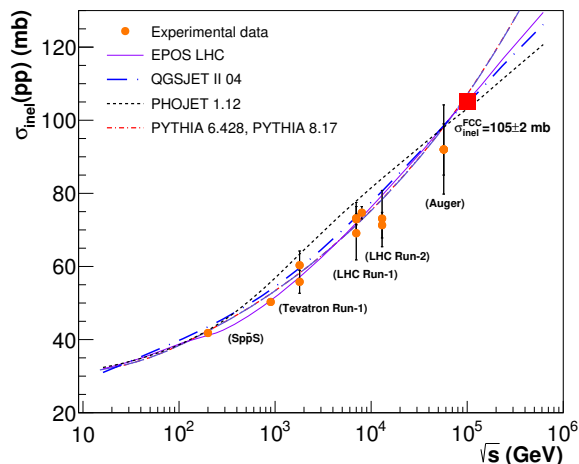
Figure 1. Inelastic p-p cross section $\sigma_{\rm inel}$ as a function of c.m. energy in the range $\sqrt{s} \approx 10\,{\rm GeV}$–$500\,{\rm TeV}$. Experimental data points at various collider and cosmic-ray energies [51–62] are compared to the predictions of EPOS-LHC, QGSJET-II-04, PHOJET 1.12, and PYTHIA (both 6.428 and 8.17 predict the same dependence). The red box indicates the average prediction of all models at $100\,{\rm TeV}$.
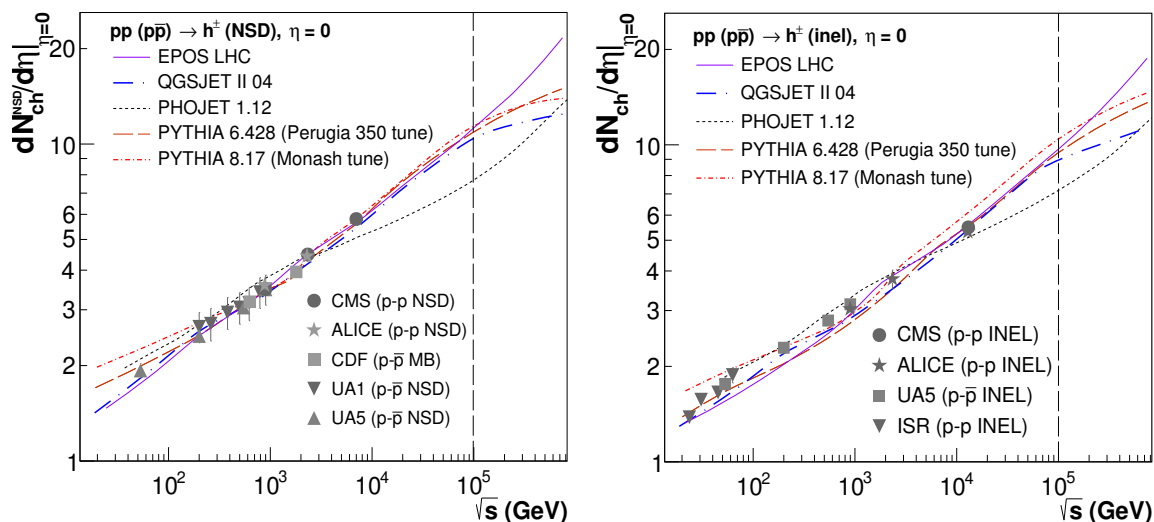
3.2 Particle pseudorapidity density

Figure 2 shows the distribution of the number of charged particles produced in p-p collisions at $100\,{\rm TeV}$ per unit of pseudorapidity as a function of pseudorapidity $(dN_{\rm ch}/d\eta)$, predicted by the different models in the range $|\eta| \lesssim 15$ (the beam *rapidity* at $\sqrt{s} = 100\,{\rm TeV}$ is $y_{\rm beam} = {\rm acosh}(\sqrt{s}/2.) \approx 11.5$). The left plot shows the NSD distribution,[2] and the right one shows the inclusive inelastic distribution which, including lower-multiplicity diffractive interactions, has a smaller average number of particles produced. All models (except PHOJET) predict about 10 charged particles at midrapidity ($\eta = 0$). Taking an unweighted average of all the predictions (except PHOJET which is systematically lower by $\sim$40%), we obtain: $dN_{\rm ch}^{\rm NSD}/d\eta|_{\eta=0} = 10.8 \pm 0.3$ and $dN_{\rm ch}/d\eta|_{\eta=0} = 9.6 \pm 0.2$. The width of the central pseudorapidity "plateau" covers $\sim$10 units from $\eta \approx -5$ to $\eta \approx +5$. At forward rapidities (equivalent to small $x \approx {\rm p_T}/\sqrt{s} \cdot {\rm e}^{-\eta}$) PYTHIA 6 and PHOJET predict noticeably "thinner" distributions than the rest, due to lower underlying gluon densities at ${\rm p_T} \approx {\rm Q_0}$, than those from the NNPDF 2.3 LO set used in PYTHIA 8 [39]. A significant fraction of the particles produced issue from the fragmentation of partons from semihard MPI, the hardest partonic collision in the MB event producing only a small fraction of them. The fact that the PHOJET particle yields are about $\sim$40% lower than the rest of MCs is indicative of missing multiparton contributions in this event generator. The c.m. energy evolution of the charged hadron pseudorapidity density at $\eta = 0$ predicted by the different models in the range $\sqrt{s} = 10\,{\rm GeV}$–$800\,{\rm TeV}$ is presented in figure 3 compared to the existing NSD (left panel) and inelastic (right panel) data measured at $\rm Sp\bar{p}S$ (UA1 [63], and UA5 [64]), Tevatron (CDF [69, 70]) and LHC (ALICE [71–73], ATLAS [65] and CMS [66–68]) colliders. The

---

[2]In PYTHIA 6 and 8 this is achieved by directly switching off single-diffractive contributions via: `MSUB(92)=MSUB(93)=0`, and `SoftQCD:singleDiffraction=off`. For PHOJET, EPOS-LHC and QGSJET-II only events MC-tagged as non-diffractive or double diffractive are included.
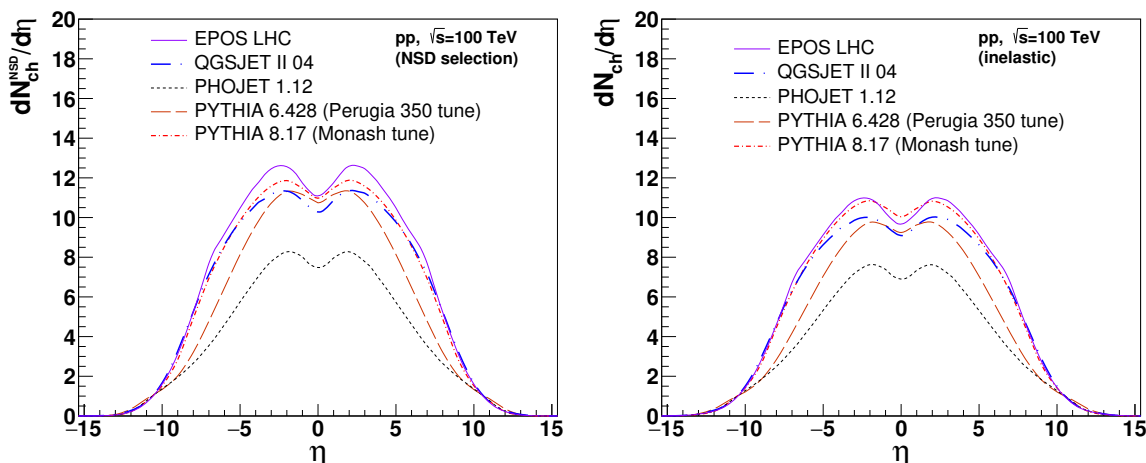
Figure 2. Distributions of the pseudorapidity density of charged particles in non single-diffractive (left) and inelastic (right) p-p collisions at $\sqrt{s} = 100\,\text{TeV}$, predicted by the different MCs considered in this work.

Figure 3. Evolution of the charged particle pseudorapidity density at midrapidity, $\text{dN}_{\text{ch}}/\text{d}\eta|_{\eta=0}$, as a function of collision energy, $\sqrt{s}$, for non-single diffractive (left) and inelastic (right) p-p collisions. The data points show existing collider data [63–68]. The vertical line indicates the FCC-hh/SppC energy at 100 TeV.

expected increase in particle multiplicity at midrapidity at 100 TeV is about a factor of two compared to the LHC results at 13 TeV ($\text{dN}_{\text{ch}}/\text{d}\eta|_{\eta=0} = 5.31 \pm 0.18$ [73], 5.49 ± 0.17 [68]). As aforementioned, the NSD selection has central densities which are about 15% larger than those obtained with the less-biased INEL trigger, which has less particles produced on average as it includes (most of) diffractive production. All models (except PHOJET, whose results are not actually trustable beyond $\sqrt{s} \approx 75\,\text{TeV}$ [74]) more or less reproduce the available experimental data up to LHC, and show a very similar trend with $\sqrt{s}$ up to FCC-hh/SppC energies. Beyond 100 TeV, however, EPOS-LHC tends to produce higher

yields than the rest of MCs. It is worth to notice that, thanks to the LHC data, the differences among model predictions have been considerably reduced in comparison to the results of the pre-LHC models discussed in [17].

The FCC-hh experiments aim at fully tracking coverage in the central $|\eta| < 5$ region. The total number of charged particles expected in the tracker system is obtained by integrating the $dN_{ch}/d\eta$ distributions over that interval, which yields an average of $N_{ch}(\Delta\eta=10) \approx 100$. For the expected FCC-hh pileups, in the range $\mathcal{O}(200-1000)$, this value implies that the trackers would sustain on average a total number of 20–100 thousand tracks per bunch crossing. Such a value is of the same order of magnitude as a *single* central Pb-Pb collision at LHC energies [75], and thus perfectly manageable for the high-granularity FCC-hh tracker designs. Further integrating the $dN_{ch}/d\eta$ distributions over all pseudorapidities, one obtains the total number of charged particles produced in an average p-p collision at 100 TeV. The EPOS, PYTHIA 8 and QGSJET-II models predict the largest total charged multiplicities, N_{ch} $(N_{ch}^{NSD}) = 161$ (184), 160 (170), 152 (172) respectively; followed by PYTHIA 6, N_{ch} $(N_{ch}^{NSD}) = 131$ (150); and PHOJET, N_{ch} $(N_{ch}^{NSD}) = 103$ (111).

## 3.3 Energy pseudorapidity density

Figure 4 shows the distributions of energy density as a function of pseudorapidity for the total energy (left) and for the energy carried by charged particles above a minimum $p_T = 100$ MeV/c (right). PHOJET predicts the lowest energy produced at all rapidities (consistent with the lower particle yields produced by the model), whereas PYTHIA 8 predicts the highest. At $\eta = 0$, the total energy produced per unit rapidity is $dE/d\eta = 9.9$, 12.2, 12.6, 13.7 and 15.6 GeV for PHOJET, QGSJET-II, PYTHIA 6, EPOS-LHC and PYTHIA 8 respectively. The same values at the forward edges of typical detector coverages ($|\eta| = 5$) are $dE/d\eta \approx 410$, 525, 670, 700 and 760 GeV for PHOJET, PYTHIA 6, QGSJET-II, EPOS-LHC and PYTHIA 8 respectively. The trend for PYTHIA 6 is to predict a smaller relative increase of energy density as a function of rapidity compared to the rest of models due, again, to a more relatively depleted underlying gluon density at the increasingly lower x values probed at forward η.

3.4 Multiplicity distribution

The multiplicity distribution $P(N_{ch})$, i.e. the probability to produce N_{ch} charged particles in a p-p event, provides important differential constraints on the internal details of the hadronic interaction models. Figure 5 shows the distribution for charged particles produced at central rapidities (within $|\eta| < 1$) in inelastic p-p collisions at the FCC-hh/SppC. The tail of the $P(N_{ch})$ distribution (right) gives information on the relative contribution of multiparton scatterings (multi-Pomeron exchanges), whereas the low multiplicity part (left) is mostly sensitive to the contributions from diffraction (single Pomeron exchanges). The various MCs considered predict quite different distributions at both ends of the spectrum. The RFT-based models EPOS-LHC and QGSJET-II predict both higher yields at very low ($N_{ch} < 3$) and very high ($N_{ch} > 100$) particle multiplicities, whereas PYTHIA 6 and 8 feature higher yields in the intermediate region $N_{ch} \approx 30$–80. PHOJET clearly produces too many particles within $N_{ch} \approx 10$–40, but much fewer at high multiplicities compared to the rest of models (which is, again, indicative of missing MPI contributions in this MC generator).
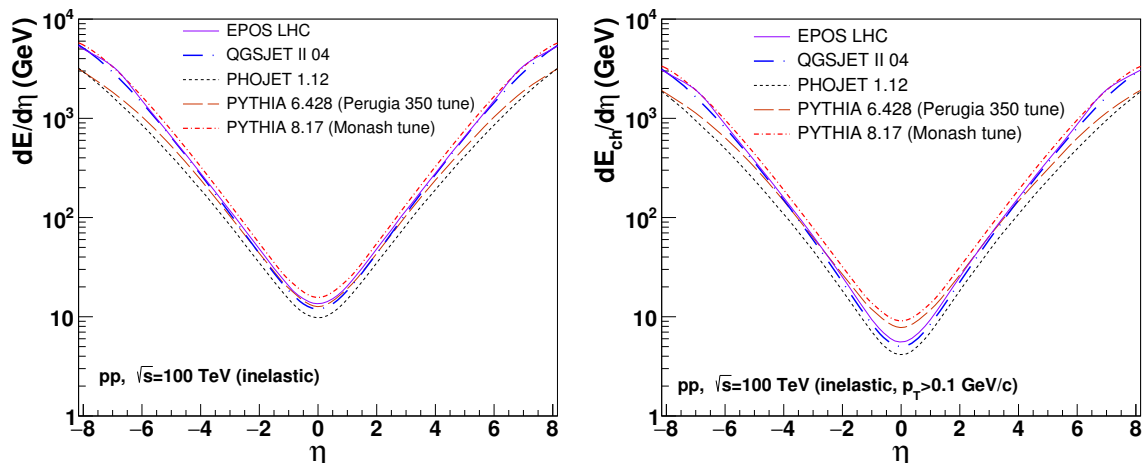
Figure 4. Distribution of the energy pseudorapidity density of all particles (left) and of charged particles with $p_T > 0.1\,\mathrm{GeV/c}$ (right) in inelastic p-p collisions at $\sqrt{s} = 100\,\mathrm{TeV}$, predicted by the different MCs considered in this work.
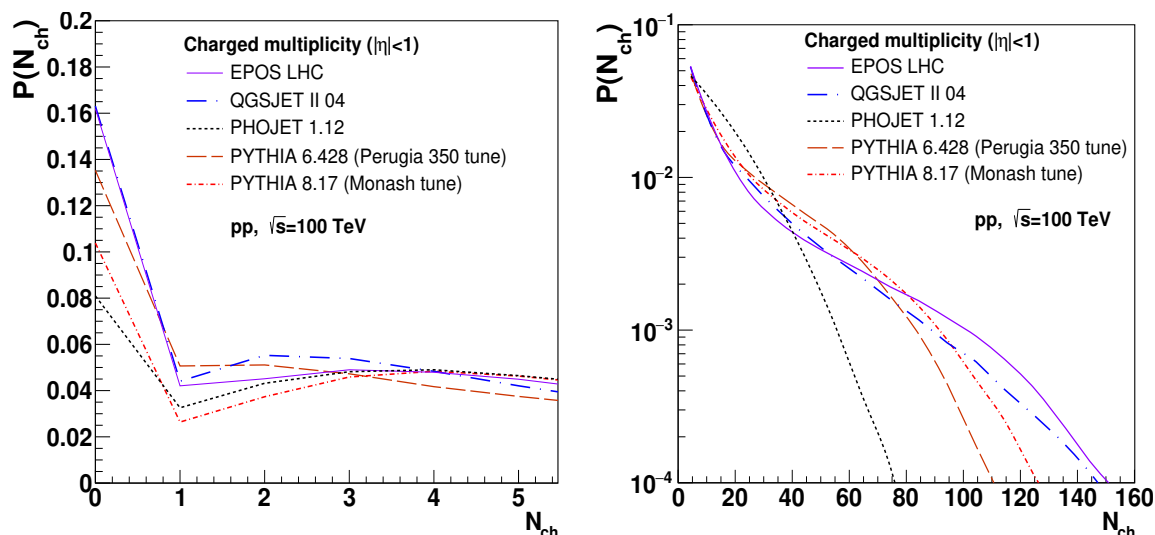
Figure 5. Per-event charged particle probability (within $|\eta| < 1$) in inelastic p-p collisions at $\sqrt{s} = 100\,\mathrm{TeV}$: full distribution (right), zoom at low multiplicities $P(N_{ch}) < 5$ (left).

3.5 Transverse momentum distribution

Figure 6 (left) shows the p_T-differential distributions of charged particles at midrapidity (within $|\eta| < 2.5$) in p-p collisions at $100\,\mathrm{TeV}$ predicted by all models. All spectra have been absolutely normalized at their value at $p_T \approx 0.5\,\mathrm{GeV/c}$ to be able to easily compare their shapes. Both PYTHIA 6 and 8 feature the largest yields at the high-p_T end of the distributions (not shown here), QGSJET-II features the "softest" spectrum, whereas EPOS shows higher yields in the region $p_T \approx 1$–$5\,\mathrm{GeV/c}$, due to collective partonic flow boosting the semihard region of the spectra, but then progressively falls below the pure-pQCD PYTHIA MC generators. The PHOJET spectrum has a more convex shape, being comparatively

– 9 –
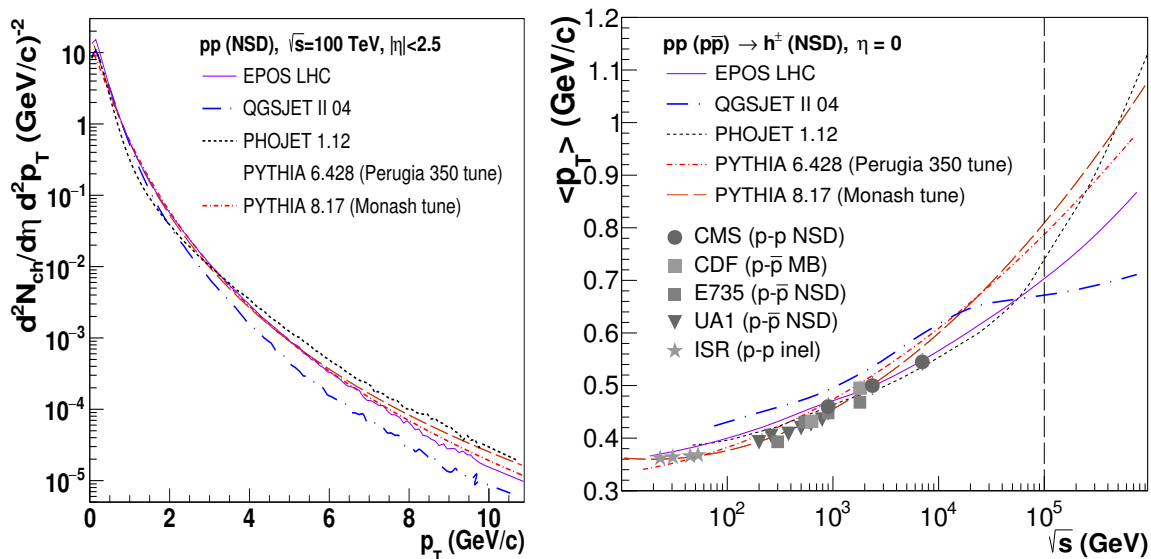
Figure 6. Left: transverse momentum spectrum in p-p collisions at $\sqrt{s} = 100\,\mathrm{TeV}$ predicted by the different MCs considered in this work (absolutely normalized at a common value at $\mathrm{p_T} \approx 0.5\,\mathrm{GeV/c}$). Right: evolution of $\langle \mathrm{p_T} \rangle$ at midrapidity as a function of c.m. energy $\sqrt{s}$. Data points show existing collider results [63, 66, 67, 70, 76, 77], and the vertical line indicates the FCC-hh/SppC energy.

depleted at intermediate $\mathrm{p_T} \approx 1$–$3\,\mathrm{GeV/c}$ but rising at its tail. Studying the $\sqrt{s}$-evolution of the average $\mathrm{p_T}$ of the spectra provides useful (integrated) information. At high energies, the peak of the perturbative cross section comes from interactions between partons whose transverse momentum is around the saturation scale, $\langle \mathrm{p_T} \rangle \approx \mathrm{Q_{sat}}$, producing (mini)jets of a few GeV which fragment into lower-$\mathrm{p_T}$ hadrons. As explained in the introduction, PYTHIA and PHOJET MCs have an energy-dependent $\mathrm{p_T}$ cutoff that mimics the power-law evolution of $\mathrm{Q_{sat}}$, while EPOS and QGSJET have a fixed $\mathrm{p_T}$ cutoff and low-x saturation is implemented through corrections to the multi-Pomeron dynamics. The different behaviours are seen in the $\sqrt{s}$-evolution of the average $\mathrm{p_T}$ shown in figure 6 (right). All MCs, but QGSJET-II, predict a (slow) power-law-like increase of $\langle \mathrm{p_T} \rangle$ with energy. Both PYTHIA 6 and 8 — whose dynamics is fully dominated by (mini)jet production — predict a higher $\langle \mathrm{p_T} \rangle$ than the rest of models, yielding $\langle \mathrm{p_T} \rangle \approx 0.82\,\mathrm{GeV/c}$ at 100 TeV to be compared with $\langle \mathrm{p_T} \rangle = 0.73$, 0.71 and $0.67\,\mathrm{GeV/c}$ from PHOJET, EPOS-LHC and QGSJET-II respectively. Above $\sqrt{s} \approx 20\,\mathrm{TeV}$, QGSJET-II predicts a flattening of $\langle \mathrm{p_T} \rangle$ whereas the EPOS-LHC evolution continues to rise due to final-state collective flow which increases $\langle \mathrm{p_T} \rangle$ with increasing multiplicity.

4 Summary

In summary, the global properties of the final states produced in hadronic interactions of protons at centre-of-mass energies of the CERN Future Circular Collider and of the IHEP Super proton-proton Collider, have been studied with various Monte Carlo event generators used in collider physics (PYTHIA 6, PYTHIA 8, and PHOJET) and in ultrahigh-energy cosmic-rays studies (EPOS, and QGSJET). Despite their different underlying modeling of hadronic

	PYTHIA 6	PYTHIA 8	EPOS-LHC	QGSJET II	PHOJET	Average*
σ_{inel} (mb)	106.9	107.1	105.4	104.8	103.1	105.1 ± 2.0
$N_{\mathrm{ch}}(N_{\mathrm{ch}}^{\mathrm{NSD}})$	131 (150)	160 (170)	161 (184)	152 (172)	101 (121)	150 (170) $\pm$ 20
$dN_{\mathrm{ch}}/d\eta|_{\eta=0}$	9.20 ± 0.01	10.10 ± 0.06	9.70 ± 0.16	9.10 ± 0.15	6.90 ± 0.13	9.6 ± 0.2
$dN_{\mathrm{ch}}^{\mathrm{NSD}}/d\eta|_{\eta=0}$	10.70 ± 0.06	10.90 ± 0.06	11.10 ± 0.18	10.30 ± 0.17	7.50 ± 0.15	10.8 ± 0.3
$dE/d\eta|_{\eta=0}$ (GeV)	12.65 ± 0.07	15.65 ± 0.02	13.70 ± 0.02	12.2 ± 0.02	9.9 ± 0.01	13.6 ± 1.5
$dE/d\eta|_{\eta=5}$ (GeV)	525 ± 4	760 ± 1	700 ± 1	670 ± 1	410 ± 1	670 ± 70
$P(N_{\mathrm{ch}} < 5)$	0.28	0.22	0.35	0.36	0.25	0.30 ± 0.03
$P(N_{\mathrm{ch}} > 100)$	$3.3 \cdot 10^{-3}$	0.011	0.025	0.018	10^{-5}	0.015 ± 0.05
$\langle p_T \rangle$ (GeV/c)	0.80 ± 0.02	0.84 ± 0.02	0.71 ± 0.02	0.67 ± 0.02	0.73 ± 0.02	0.76 ± 0.07

Table 3. Comparison of the basic properties of particle production in p-p collisions at $\sqrt{s} = 100 \, \mathrm{TeV}$, predicted by PYTHIA 6 and 8, EPOS-LHC, QGSJET-II, and PHOJET: inelastic cross section σ_{inel}; total charged multiplicities (N_{ch}), and pseudorapidity charged particle densities at midrapidity ($dN_{\mathrm{ch}}/d\eta|_{\eta=0}$) for inelastic and NSD selections; energy densities at midrapidity ($dE/d\eta|_{\eta=0}$), and at more forward rapidities ($dE/d\eta|_{\eta=5}$); typical values of the charged multiplicity probabilities $P(N_{\mathrm{ch}})$ (over $|\eta| < 1$) for low and high values of N_{ch}; and mean charged particle transverse momentum $\langle p_T \rangle$ over $|\eta| < 2.5$. The quoted uncertainties on the individual predictions are just the MC statistical ones. The last column indicates the average of all MCs (except PHOJET)* for each observable, with uncertainties approximately covering the range of the predictions.

interactions, their predictions for proton-proton collisions at $\sqrt{s} = 100 \, \mathrm{TeV}$ are quite similar (excluding PHOJET, whose parameters have not been retuned with the collider data in the last 15 years). Table 3 lists the basic kinematical observables predicted for p-p at 100 TeV by all MC generators considered.

The averages of all MC predictions (except PHOJET) for the different observables are: (i) p-p inelastic cross sections $\sigma_{\mathrm{inel}} = 105 \pm 2$ mb (to be compared with $\sigma_{\mathrm{inel}} \approx 72$ mb at the LHC(13 TeV), i.e. a $\sim$45% increase), (ii) total charged multiplicity N_{ch} ($N_{\mathrm{ch}}^{\mathrm{NSD}}$) = 150 (170) $\pm$ 20, (iii) charged particle pseudorapidity density at midrapidity $dN_{\mathrm{ch}}/d\eta|_{\eta=0} = 9.6 \pm 0.2$ (to be compared with the LHC(13 TeV) result of $dN_{\mathrm{ch}}/d\eta|_{\eta=0} = 5.4 \pm 0.2$, i.e. an increase of $\sim$80%), and $dN_{\mathrm{ch}}^{\mathrm{NSD}}/d\eta|_{\eta=0} = 10.8 \pm 0.3$ for the NSD selection, (iv) energy density at midrapidity $dE/d\eta|_{\eta=0} = 13.6 \pm 1.5 \, \mathrm{GeV}$, and energy density at the edge of the central region $dE/d\eta|_{\eta=5} = 670 \pm 70 \, \mathrm{GeV}$, and (v) average transverse momenta at midrapidities $\langle p_T \rangle = 0.76 \pm 0.07 \, \mathrm{GeV/c}$ (to be compared with $\langle p_T \rangle = 0.55 \pm 0.16 \, \mathrm{GeV/c}$ at the LHC(8 TeV), i.e. a $\sim$40% increase). The per-event multiplicity probabilities $P(N_{\mathrm{ch}})$, have been also compared: EPOS-LHC and QGSJET-II both predict higher yields at very low ($N_{\mathrm{ch}} < 3$) and very high ($N_{\mathrm{ch}} > 100$) particle multiplicities, whereas PYTHIA 6 and 8 feature higher yields in the intermediate region $N_{\mathrm{ch}} \approx 30$–80. These results are useful to estimate the expected detector occupancies and energy deposits from pileup collisions at high luminosities of relevance for planned FCC-hh/SppC detector designs.

Acknowledgments

References

[1] T. Golling et al., *Physics at a 100 TeV pp collider: beyond the Standard Model phenomena*, [CERN-TH-2016-111](#) [[arXiv:1606.00947](#)] [[INSPIRE](#)].

[2] M.L. Mangano et al., *Physics at a 100 TeV pp collider: Standard Model processes*, [CERN-TH-2016-112](#) [[arXiv:1607.01831](#)] [[INSPIRE](#)].

[3] R. Contino et al., *Physics at a 100 TeV pp collider: Higgs and EW symmetry breaking studies*, [CERN-TH-2016-113](#) [[arXiv:1606.09408](#)] [[INSPIRE](#)].

[4] M. Benedikt, B. Goddard, D. Schulte, F. Zimmermann and M.J. Syphers, *FCC-hh Hadron Collider — Parameter Scenarios and Staging Options*, in proceedings of *6th International Particle Accelerator Conference (IPAC2015)*, Richmond, VA, U.S.A., IPAC-2015-TUPTY062.

[5] CEPC-SPPC Study Group collaboration, *CEPC-SPPC Preliminary Conceptual Design Report. 1. Physics and Detector*, [[INSPIRE](#)]

[6] V.N. Gribov and L.N. Lipatov, *Deep inelastic e p scattering in perturbation theory*, *Sov. J. Nucl. Phys.* **15** (1972) 438 [[INSPIRE](#)].

[7] G. Altarelli and G. Parisi, *Asymptotic Freedom in Parton Language*, [*Nucl. Phys.* **B 126** (1977) 298](#) [[INSPIRE](#)].

[8] Y.L. Dokshitzer, *Calculation of the Structure Functions for Deep Inelastic Scattering and e^+e^- Annihilation by Perturbation Theory in Quantum Chromodynamics.*, *Sov. Phys. JETP* **46** (1977) 641 [[INSPIRE](#)].

[9] V.N. Gribov, *A reggeon diagram technique*, *Sov. Phys. JETP* **26** (1968) 414 [[INSPIRE](#)].

[10] A. Capella, U. Sukhatme, C.-I. Tan and J. Tran Thanh Van, *Dual parton model*, [*Phys. Rept.* **236** (1994) 225](#) [[INSPIRE](#)].

[11] S. Donnachie, H.G. Dosch, O. Nachtmann and P. Landshoff, *Pomeron physics and QCD*, *Camb. Monogr. Part. Phys. Nucl. Phys. Cosmol.* **19** (2002) 1 [[INSPIRE](#)].

[12] CMS collaboration, *Measurement of diffraction dissociation cross sections in pp collisions at $\sqrt{s} = 7$ TeV*, [*Phys. Rev.* **D 92** (2015) 012003](#) [[arXiv:1503.08689](#)] [[INSPIRE](#)].

[13] T. Sjöstrand, S. Mrenna and P.Z. Skands, *PYTHIA 6.4 Physics and Manual*, [*JHEP* **05** (2006) 026](#) [[hep-ph/0603175](#)] [[INSPIRE](#)].

[14] T. Sjöstrand, S. Mrenna and P.Z. Skands, *A Brief Introduction to PYTHIA 8.1*, [*Comput. Phys. Commun.* **178** (2008) 852](#) [[arXiv:0710.3820](#)] [[INSPIRE](#)].

[15] M. Bahr et al., *HERWIG++ Physics and Manual*, [*Eur. Phys. J.* **C 58** (2008) 639](#) [[arXiv:0803.0883](#)] [[INSPIRE](#)].

[16] T. Gleisberg et al., *Event generation with SHERPA 1.1*, [*JHEP* **02** (2009) 007](#) [[arXiv:0811.4622](#)] [[INSPIRE](#)].

[17] D. d'Enterria, R. Engel, T. Pierog, S. Ostapchenko and K. Werner, *Constraints from the first LHC data on hadronic event generators for ultra-high energy cosmic-ray physics*, *Astropart. Phys.* **35** (2011) 98 [`arXiv:1101.5596`] [ɪɴSPIRE].

[18] K. Werner, F.-M. Liu and T. Pierog, *Parton ladder splitting and the rapidity dependence of transverse momentum spectra in deuteron-gold collisions at RHIC*, *Phys. Rev.* **C 74** (2006) 044902 [`hep-ph/0506232`] [ɪɴSPIRE].

[19] T. Pierog and K. Werner, *EPOS Model and Ultra High Energy Cosmic Rays*, *Nucl. Phys. Proc. Suppl.* **196** (2009) 102 [`arXiv:0905.1198`] [ɪɴSPIRE].

[20] T. Pierog, I. Karpenko, J.M. Katzy, E. Yatsenko and K. Werner, *EPOS LHC: Test of collective hadronization with data measured at the CERN Large Hadron Collider*, *Phys. Rev.* **C 92** (2015) 034906 [`arXiv:1306.0121`] [ɪɴSPIRE].

[21] N.N. Kalmykov and S.S. Ostapchenko, *The nucleus-nucleus interaction, nuclear fragmentation and fluctuations of extensive air showers*, *Phys. Atom. Nucl.* **56** (1993) 346 [ɪɴSPIRE].

[22] N.N. Kalmykov, S.S. Ostapchenko and A.I. Pavlov, *quark-gluon String Model and EAS Simulation Problems at Ultra-High Energies*, *Nucl. Phys. Proc. Suppl.* **52** (1997) 17 [ɪɴSPIRE].

[23] S. Ostapchenko, *Nonlinear screening effects in high energy hadronic interactions*, *Phys. Rev.* **D 74** (2006) 014026 [`hep-ph/0505259`] [ɪɴSPIRE].

[24] S. Ostapchenko, *QGSJET-II: Towards reliable description of very high energy hadronic interactions*, *Nucl. Phys. Proc. Suppl.* **151** (2006) 143 [`hep-ph/0412332`] [ɪɴSPIRE].

[25] S. Ostapchenko, *Status of QGSJET*, *AIP Conf. Proc.* **928** (2007) 118 [`arXiv:0706.3784`] [ɪɴSPIRE].

[26] S. Ostapchenko, *Monte Carlo treatment of hadronic interactions in enhanced Pomeron scheme: I. QGSJET-II model*, *Phys. Rev.* **D 83** (2011) 014018 [`arXiv:1010.1869`] [ɪɴSPIRE].

[27] E.-J. Ahn, R. Engel, T.K. Gaisser, P. Lipari and T. Stanev, *Cosmic ray interaction event generator SIBYLL 2.1*, *Phys. Rev.* **D 80** (2009) 094003 [`arXiv:0906.4113`] [ɪɴSPIRE].

[28] R. Engel, *Photoproduction within the two component dual parton model. 1. Amplitudes and cross-sections*, *Z. Phys.* **C 66** (1995) 203 [ɪɴSPIRE].

[29] R. Engel and J. Ranft, *Hadronic photon-photon interactions at high-energies*, *Phys. Rev.* **D 54** (1996) 4244 [`hep-ph/9509373`] [ɪɴSPIRE].

[30] R. Engel, J. Ranft and S. Roesler, *Hard diffraction in hadron hadron interactions and in photoproduction*, *Phys. Rev.* **D 52** (1995) 1459 [`hep-ph/9502319`] [ɪɴSPIRE].

[31] T. Sjöstrand and M. van Zijl, *A Multiple Interaction Model for the Event Structure in Hadron Collisions*, *Phys. Rev.* **D 36** (1987) 2019 [ɪɴSPIRE].

[32] L.V. Gribov, E.M. Levin and M.G. Ryskin, *Semihard Processes in QCD*, *Phys. Rept.* **100** (1983) 1 [ɪɴSPIRE].

[33] B. Andersson, G. Gustafson, G. Ingelman and T. Sjöstrand, *Parton Fragmentation and String Dynamics*, *Phys. Rept.* **97** (1983) 31 [ɪɴSPIRE].

[34] X. Artru and G. Mennessier, *String model and multiproduction*, *Nucl. Phys.* **B 70** (1974) 93 [ɪɴSPIRE].

[35] G. Marchesini, B.R. Webber, G. Abbiendi, I.G. Knowles, M.H. Seymour and L. Stanco, *HERWIG 5.1 — A Monte Carlo event generator for simulating hadron emission reactions with interfering gluons*, *Comput. Phys. Commun.* **67** (1992) 465 [INSPIRE].

[36] D. Bourilkov, R.C. Group and M.R. Whalley, *LHAPDF: PDF use from the Tevatron to the LHC*, hep-ph/0605240 [INSPIRE].

[37] G.A. Schuler and T. Sjöstrand, *Hadronic diffractive cross-sections and the rise of the total cross-section*, *Phys. Rev.* **D 49** (1994) 2257 [INSPIRE].

[38] P.Z. Skands, *Tuning Monte Carlo Generators: The Perugia Tunes*, *Phys. Rev.* **D 82** (2010) 074018 [arXiv:1005.3457] [INSPIRE].

[39] P. Skands, S. Carrazza and J. Rojo, *Tuning PYTHIA 8.1: the Monash 2013 Tune*, *Eur. Phys. J.* **C 74** (2014) 3024 [arXiv:1404.5630] [INSPIRE].

[40] C.O. Rasmussen, *Hard Diffraction in PYTHIA 8*, *EPJ Web Conf.* **120** (2016) 02002 [arXiv:1512.05872] [INSPIRE].

[41] CTEQ collaboration, H.L. Lai et al., *Global QCD analysis of parton structure of the nucleon: CTEQ5 parton distributions*, *Eur. Phys. J.* **C 12** (2000) 375 [hep-ph/9903282] [INSPIRE].

[42] NNPDF collaboration, R.D. Ball et al., *Parton distributions with QED corrections*, *Nucl. Phys.* **B 877** (2013) 290 [arXiv:1308.0598] [INSPIRE].

[43] P.Z. Skands and D. Wicke, *Non-perturbative QCD effects and the top mass at the Tevatron*, *Eur. Phys. J.* **C 52** (2007) 133 [hep-ph/0703081] [INSPIRE].

[44] T. Sjöstrand et al., *An introduction to PYTHIA 8.2*, *Comput. Phys. Commun.* **191** (2015) 159 [arXiv:1410.3012] [INSPIRE].

[45] H.J. Drescher, M. Hladik, S. Ostapchenko, T. Pierog and K. Werner, *Parton based Gribov-Regge theory*, *Phys. Rept.* **350** (2001) 93 [hep-ph/0007198] [INSPIRE].

[46] S. Ostapchenko, *On the re-summation of enhanced Pomeron diagrams*, *Phys. Lett.* **B 636** (2006) 40 [hep-ph/0602139] [INSPIRE].

[47] S. Ostapchenko, *Enhanced Pomeron diagrams: Re-summation of unitarity cuts*, *Phys. Rev.* **D 77** (2008) 034009 [hep-ph/0612175] [INSPIRE].

[48] S. Ostapchenko, *Non-linear effects in high energy hadronic interactions*, hep-ph/0501093 [INSPIRE].

[49] M.L. Good and W.D. Walker, *Diffraction disssociation of beam particles*, *Phys. Rev.* **120** (1960) 1857 [INSPIRE].

[50] A. Donnachie and P.V. Landshoff, *Total cross-sections*, *Phys. Lett.* **B 296** (1992) 227 [hep-ph/9209205] [INSPIRE].

[51] UA5 collaboration, G.J. Alner et al., *Antiproton-proton cross sections at 200 and 900 GeV c.m. energy*, *Z. Phys.* **C 32** (1986) 153 [INSPIRE].

[52] E710 collaboration, N.A. Amos et al., *Measurement of ρ, the ratio of the real to imaginary part of the $\bar{p}p$ forward elastic scattering amplitude, at $\sqrt{s} = 1.8$ TeV*, *Phys. Rev. Lett.* **68** (1992) 2433 [INSPIRE].

[53] CDF collaboration, F. Abe et al., *Measurement of the $\bar{p}p$ total cross-section at $\sqrt{s} = 546$ GeV and 1800 GeV*, *Phys. Rev.* **D 50** (1994) 5550 [INSPIRE].

[54] ALICE collaboration, *Measurement of inelastic, single- and double-diffraction cross sections in proton-proton collisions at the LHC with ALICE*, *Eur. Phys. J.* **C 73** (2013) 2456 [arXiv:1208.4968] [INSPIRE].

[55] ATLAS collaboration, *Measurement of the Inelastic Proton-Proton Cross-Section at $\sqrt{s} = 7\,TeV$ with the ATLAS Detector*, *Nature Commun.* **2** (2011) 463 [arXiv:1104.0326] [INSPIRE].

[56] ATLAS collaboration, *Measurement of the Inelastic Proton-Proton Cross section at $\sqrt{s} = 13\,TeV$ with the ATLAS Detector at the LHC*, ATLAS-CONF-2015-038.

[57] CMS collaboration, *Measurement of the inelastic proton-proton cross section at $\sqrt{s} = 7\,TeV$*, *Phys. Lett.* **B 722** (2013) 5 [arXiv:1210.6718] [INSPIRE].

[58] CMS collaboration, *Measurement of diffractive dissociation cross sections in pp collisions at $\sqrt{s} = 7\,TeV$*, CMS-FSQ-2015-005.

[59] G. Antchev et al., *First measurement of the total proton-proton cross section at the LHC energy of $\sqrt{s} = 7\,TeV$*, *Europhys. Lett.* **96** (2011) 21002 [arXiv:1110.1395] [INSPIRE].

[60] TOTEM collaboration, G. Antchev et al., *Luminosity-independent measurements of total, elastic and inelastic cross-sections at $\sqrt{s} = 7\,TeV$*, *Europhys. Lett.* **101** (2013) 21004 [INSPIRE].

[61] TOTEM collaboration, G. Antchev et al., *Luminosity-Independent Measurement of the Proton-Proton Total Cross section at $\sqrt{s} = 8\,TeV$*, *Phys. Rev. Lett.* **111** (2013) 012001 [INSPIRE].

[62] PIERRE AUGER collaboration, P. Abreu et al., *Measurement of the proton-air cross-section at $\sqrt{s} = 57\,TeV$ with the Pierre Auger Observatory*, *Phys. Rev. Lett.* **109** (2012) 062002 [arXiv:1208.1520] [INSPIRE].

[63] UA1 collaboration, C. Albajar et al., *A Study of the General Characteristics of $p\bar{p}$ Collisions at $\sqrt{s} = 0.2\,TeV$ to $0.9\,TeV$*, *Nucl. Phys.* **B 335** (1990) 261 [INSPIRE].

[64] UA5 collaboration, G.J. Alner et al., *Scaling of Pseudorapidity Distributions at c.m. Energies Up to $0.9\,TeV$*, *Z. Phys.* **C 33** (1986) 1 [INSPIRE].

[65] ATLAS collaboration, *Charged-particle multiplicities in pp interactions measured with the ATLAS detector at the LHC*, *New J. Phys.* **13** (2011) 053033 [arXiv:1012.5104] [INSPIRE].

[66] CMS collaboration, *Transverse momentum and pseudorapidity distributions of charged hadrons in pp collisions at $\sqrt{s} = 0.9$ and $2.36\,TeV$*, *JHEP* **02** (2010) 041 [arXiv:1002.0621] [INSPIRE].

[67] CMS collaboration, *Transverse-momentum and pseudorapidity distributions of charged hadrons in pp collisions at $\sqrt{s} = 7\,TeV$*, *Phys. Rev. Lett.* **105** (2010) 022002 [arXiv:1005.3299] [INSPIRE].

[68] CMS collaboration, *Pseudorapidity distribution of charged hadrons in proton-proton collisions at $\sqrt{s} = 13\,TeV$*, *Phys. Lett.* **B 751** (2015) 143 [arXiv:1507.05915] [INSPIRE].

[69] CDF collaboration, F. Abe et al., *Pseudorapidity distributions of charged particles produced in $\bar{p}p$ interactions at $\sqrt{s} = 630\,GeV$ and $1800\,GeV$*, *Phys. Rev.* **D 41** (1990) 2330 [INSPIRE].

[70] CDF collaboration, F. Abe et al., *Transverse Momentum Distributions of Charged Particles Produced in $\bar{p}p$ Interactions at $\sqrt{s} = 630\,GeV$ and $1800\,GeV$*, *Phys. Rev. Lett.* **61** (1988) 1819 [INSPIRE].

[71] ALICE collaboration, *Charged-particle multiplicity measurement in proton-proton collisions at $\sqrt{s} = 0.9$ and 2.36 TeV with ALICE at LHC*, *Eur. Phys. J.* **C 68** (2010) 89 [arXiv:1004.3034] [INSPIRE].

[72] ALICE collaboration, *Charged-particle multiplicity measurement in proton-proton collisions at $\sqrt{s} = 7$ TeV with ALICE at LHC*, *Eur. Phys. J.* **C 68** (2010) 345 [arXiv:1004.3514] [INSPIRE].

[73] ALICE collaboration, *Pseudorapidity and transverse-momentum distributions of charged particles in proton-proton collisions at $\sqrt{s} = 13$ TeV*, *Phys. Lett.* **B 753** (2016) 319 [arXiv:1509.08734] [INSPIRE].

[74] R. Engel, private communication.

[75] ALICE collaboration, *Centrality dependence of the charged-particle multiplicity density at midrapidity in Pb-Pb collisions at $\sqrt{s_{\mathrm{NN}}} = 5.02$ TeV*, *Phys. Rev. Lett.* **116** (2016) 222302 [arXiv:1512.06104] [INSPIRE].

[76] A.M. Rossi, G. Vannini, A. Bussiere, E. Albini, D. D'Alessandro and G. Giacomelli, *Experimental Study of the Energy Dependence in Proton Proton Inclusive Reactions*, *Nucl. Phys.* **B 84** (1975) 269 [INSPIRE].

[77] T. Alexopoulos et al., *Multiplicity Dependence of the Transverse Momentum Spectrum for Centrally Produced Hadrons in Antiproton-Proton Collisions at $\sqrt{s} = 1.8$ TeV*, *Phys. Rev. Lett.* **60** (1988) 1622 [INSPIRE].